A time-saving and cost-effective method to process alloys by Laser Powder Bed Fusion

Elsevier Editorial System(tm) for Materials and Design

Manuscript Draft

Manuscript Number:

Title: A time-saving and cost-effective method to process new alloys by Laser Powder Bed Fusion

Article Type: Research Paper

Keywords: Laser Powder Bed Fusion (LPBF); Single scan tracks (SSTs); Hatching distance; Overlap; Time-saving method; Process parameters optimization

Corresponding Author: Mr. Federico Bosio, Ph.D.

Corresponding Author's Institution: Politecnico di Torino

First Author: Federico Bosio, Ph.D.

Order of Authors: Federico Bosio, Ph.D.; Alberta Aversa; Massimo Lorusso; Silvia Marola; Dario Gianoglio; Livio Battezzati; Paolo Fino; Diego Manfredi; Mariangela Lombardi

Abstract: Additive manufacturing (AM), and in particular Laser Powder Bed Fusion (LPBF), opens completely new possibilities to produce novel alloy compositions.
Optimization of the main process parameters is a core procedure while developing novel alloy compositions for LPBF. To that aim, traditional Design Of Experiment (DOE) approaches have been widely used to determine the operating process windows through the manufacturing of several matrices of massive samples. However, considering the high cost of spherical gas-atomized powders, this represents a time consuming and expensive route.
In this work, a novel method to quickly manufacture dense samples of new alloys through LPBF is proposed. This method was applied on an aluminum alloy system obtained mixing AlSi10Mg and Cu powders. At first, a power (P)- speed (v) operating window is easily defined by means of Single Scan Tracks (SSTs). Then, the proper hatching distance (hd) is designed considering to have an optimum overlap among adjacent scan tracks. In this way, massive samples can be directly produced by using the best P-v-hd combinations, avoiding many experiments. Finally, a scenario of hardness and productivity vs. energy density is given for the investigated AlSi10Mg+4Cu alloy, in order to find the optimum compromise between mechanical properties and industrial needs.

Cover Letter

POLITECNICO DI TORINO
Dipartimento
di Scienza Applicata
e Tecnologia

Torino, 23/03/2019

Dear Editor,

we kindly ask you to consider the submission of our manuscript entitled "A time-saving and cost-effective method to produce new alloys for Laser Powder Bed Fusion" for publication as Research Article in *Materials & Design*.

The main aim of this study is to define a time- and cost-effective method to process new alloy compositions by Laser Powder Bed Fusion. The novelty of the proposed approach relies in the ability to set at level of single laser scan tracks the main process parameters, i.e. laser power (P), scanning speed (v) and hatching distance (h_d), to produce dense samples, saving time and starting powders.

The definition of the main process parameters for a AlSi10Mg+4Cu system obtained by mixing allows us to set-up a novel method to produce near fully dense massive samples by means of few steps. Firstly, a reliable P-v operating window is easily defined analysing single scan tracks. Secondly, the proper h_d can be designed considering the grade of overlap between nearby single tracks. Finally, massive samples are directly produced by using the optimum P-v combinations, the designed h_d and the desired scanning strategy, avoiding time-consuming DOE experiments.

It was demonstrated that the method can be exploited for every LPBF powders, considering gas-atomized or mixed ones, as verified also in the case of the AlSi10Mg alloy.

This manuscript presents original work and is not under consideration by any other journal. All authors approved the manuscript and this submission.

Thank you for considering our manuscript for review. We look forward to your response.

Sincerely yours,

Federico Bosio

Materials Engineer, Ph.D Candidate
Department of Applied Science and Technology (DISAT), Politecnico di Torino
Address: Corso Duca degli Abruzzi 24, 10129, Torino, Italy
Mobile Phone: 0478 153 835
E-Mail: federico.bosio@polito.it

*Graphical Abstract

New alloys for LPBF

Single Scan Tracks analysis

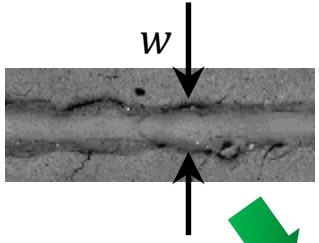

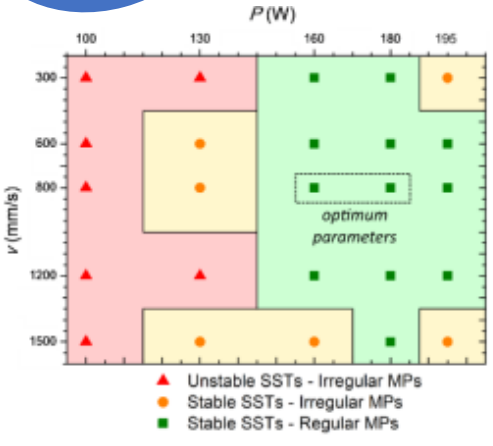

$$h_d = w \cdot \left(1 - \frac{\varphi}{100}\right)$$

$$0\ \% \leq \varphi \leq 20\ \%$$

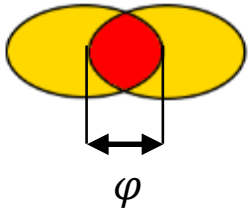

$$\boldsymbol{Defined}\ \boldsymbol{P, v, h_d}$$

Dense samples

Highlights (for review)

- A time- and cost- effective method to manufacture new alloys by Laser Powder Bed Fusion (LPBF) is proposed.
- The definition of main process parameters for processing new alloys for LPBF is achieved by means of Single Scan Tracks (SSTs).
- A proper overlap between nearby SSTs is the key for defining the proper hatching distance for high density massive samples.
- A scenario of hardness and productivity vs. energy density is given for a new Al alloy: AlSi10Mg + 4wt % Cu mixed alloy.

A time-saving and cost-effective method to process new alloys by Laser Powder Bed Fusion

Federico Bosio[1*], Alberta Aversa[1], Massimo Lorusso[2], Silvia Marola[3], Dario Gianoglio[3], Livio Battezzati[3], Paolo Fino[1], Diego Manfredi[2], Mariangela Lombardi[1]

[1] Department of Applied Science and Technology, Politecnico di Torino, Corso Duca degli Abruzzi 24, 10129 Torino, Italy;
[2] Center for Sustainable Future Technologies CSFT@Polito, Istituto Italiano di Tecnologia, Via Livorno 60, 10144 Torino, Italy;
[3] Dipartimento di Chimica, Università di Torino, Torino, Italy.
*Corresponding author: Email: federico.bosio@polito.it
Postal address: Corso Duca degli Abruzzi 24, 10129, Politecnico di Torino, Torino, Italy.

Abstract

Additive manufacturing (AM), and in particular Laser Powder Bed Fusion (LPBF), opens completely new possibilities to produce novel alloy compositions.

Optimization of the main process parameters is a core procedure while developing novel alloy compositions for LPBF. To that aim, traditional Design Of Experiment (DOE) approaches have been widely used to determine the operating process windows through the manufacturing of several matrices of massive samples. However, considering the high cost of spherical gas-atomized powders, this represents a time consuming and expensive route.

In this work, a novel method to quickly manufacture dense samples of new alloys through LPBF is proposed. This method was applied on an aluminum alloy system obtained mixing AlSi10Mg and Cu powders. At first, a power (*P*) – speed (*v*) operating window is easily defined by means of Single Scan Tracks (SSTs). Then, the proper hatching distance (h_d) is designed considering to have an optimum overlap among adjacent scan tracks. In this way, massive samples can be directly produced by using the best *P*-*v*-h_d combinations, avoiding many experiments. Finally, a scenario of hardness and productivity vs. energy density is given for the investigated AlSi10Mg+4Cu alloy, in order to find the optimum compromise between mechanical properties and industrial needs.

Keywords

Laser Powder Bed Fusion (LPBF), Single scan tracks (SSTs), Hatching distance (h_d), Overlap, Time-saving method, Process parameters optimization, Productivity.

1. Introduction

Additive manufacturing (AM) of metal parts is widely recognized as a “powerful” alternative to conventional casting route for medium-low batch production, thanks to its capability to manufacture complex shaped parts with high design freedom and without the presence of joints or welds [1]. AM is considered a strategic technology and a key enabler for accelerated engineering processes. Moreover, metallic AM opens completely new opportunities to design novel alloy compositions with specific properties which cannot be generated in conventional processes, due to the peculiar conditions similar to those of rapid solidification processes [2]. Among AM techniques for metals, Laser Powder Bed Fusion (LPBF) has been extensively used during the last decade [3]. This process is also known as Selective Laser Melting (SLM), but now this term is associated to the use of a specific commercial machine (SLM Solutions, Germany). Nowadays, there have been only a limited number of alloy systems available in the marketplace for LPBF, the most widespread being pure titanium and Ti6Al4V alloy, stainless steels, nickel-based superalloys, Al-Si casting alloys, cobalt-chromium and recently high-entropy alloys [4–11]. Therefore, to exploit all the benefits of LPBF, developing new alloy compositions of industrial interest is now becoming a key challenge to address in the field [12].

However, the development of new alloys for LPBF is not a simple route and, generally, requires important economical efforts. As an example, the high cost of the starting powder can significantly increase the price of final parts: powder costs are the second largest cost associated with producing LPBF parts [13]. In fact, as a rule for all

powder bed systems, highly spherical gas-atomized powders with specific particle size distribution are required to guarantee good flowability and to prevent the formation of porosities [14,15]. Actually, the number of companies able to gas atomize such powders is not too high. For this reason, when a novel metal system is investigated, one might need an ad-hoc customized powder which is rather expensive and quite difficult to be purchased on the market in a short time.

Once the suitable powder is produced, optimization of the main process parameters is a core procedure for developing novel compositions for LPBF. In this respect, the main goal is to reach the highest level of density, possibly near the theoretical one. Actually, there are many process parameters to be tuned that can affect the layer by layer adhesion with a direct influence on mechanical properties of the parts. The main process parameters are laser power (*P*), scan speed (*v*), hatching distance (h_d) and scanning strategy [16]. The hatching distance is the distance between consecutive laser passes, while the scanning strategy is related to the path followed by the laser in each layer. To that aim, traditional Design Of Experiment (DOE) approaches, such as full factorial design [17], two-level fractional factorial design [18] and response surface method [19], have been widely used to determine the operating window of well-known alloys directly through the production of matrices of massive samples, like cubes or parallelepipeds. Despite the successful results that can be obtained using these approaches, the production of a great number of specimens and time-intensive experiments are required [17–20]. Hence, considering the high usage of powder and the working time for samples production, this approach means also high costs.

Conversely, recent findings in literature demonstrated that the operating window for LPBF of an alloy can be also determined via the Single Scan Tracks (SSTs) approach, which requires very small quantity of powders with respect to the manufacturing of massive samples [9,21–26]. It can be stated that in the LPBF process, each section of a component is filled by nearby single scan tracks under the laser heating, the so-called hatching lines. Therefore the quality of the manufactured parts is strictly related to the properties of each single track. For example, considering Ni-based superalloys, Li et al. identified the operating window of Inconel 625 according to SSTs characteristics [23]. They observed that defects and porosity were more prone to form in tracks built at high laser power due to the turbulence of the melt pool, being the melt pool the cross-section of a single laser scan track. Considering Al alloys, Kempen et al. observed that the highest densities of AlSi10Mg parts produced by SLM are reached when the Linear Energy Density (LED) is optimal to produce regular tracks with stable melt pool [9]. In agreement with this, in a recent study, Wei et al. showed that the large amount of pores in SLM*ed* AlSi10Mg samples built with a parameters combination corresponding to a low Volumetric Energy Density (VED) are mainly caused by the discontinuous scan track used in the manufacturing [24].

In other studies on AlSi10Mg alloys, it was also highlighted the importance of the hatching distance parameter, defined by the laser spot size and by the laser-powder interaction. It is well-documented that a proper overlap between nearby single tracks is fundamental to prevent the formation of porosities [17,19,27]. Each result of these studies depends on the LPBF system employed, and on the main parameters adopted. However, as a general rule, it can be stated that the increase in h_d reduces the overlapping of neighbouring single tracks and increases porosity. The h_d represents, therefore, the link between SSTs and building strategy for massive samples production by LPBF.

Recently, Nie et al. studied the effect of processing parameters on the formation of single scan track, multi-tracks and cubic samples for a SLMed Al-Cu-Mg alloy [26]. For the specific alloy selected for their work, once the optimal processing windows were obtained, they analyzed microstructures and related mechanical properties.

The main aim of this study is to define a time- and cost-effective innovative method to manufacture new alloys for LPBF. At first, SSTs are performed by using mixed powders, cheaper than gas-atomized ones with a customized composition. Once obtained continuous and stable SSTs, controlled by *P* and *v*, the measurement of their mean track width allows to select directly the optimum h_d value to ensure a good overlapping and, therefore, the manufacturing of dense samples. In all the previous mentioned studies, it is still problematic to determine a-priori an h_d without employing time and cost consuming experiments. Therefore, the novelty of the proposed approach relies in the ability to define the main process parameters to produce dense samples already at level of SSTs.

In this study, the starting powders are AlSi10Mg + 4% wt. Cu obtained by simply mixing, but the method can be exploited for every LPBF powder, considering gas-atomized or mixed ones, as demonstrated in the discussion section also through the case of the AlSi10Mg alloy.

2. Materials and Methods

2.1 Raw material

Pre-alloyed gas atomized powder of AlSi10Mg and high chemical pure Cu (HCP Cu) powder, supplied respectively by EOS Gmbh and Sandvik Osprey LTD, were mixed for 24 h at a speed of 60 rpm by using ceramic jars without grinding media. This mixing technique was adopted in order to avoid the deformation of the starting powder and preserve its flowability. The chemical composition of the starting powders together with the calculated AlSi10Mg+4Cu alloy composition are summarized in Table 1. The mixed powder was firstly investigated by means of a Field Emission Scanning Electron Microscope (FESEM) Zeiss SupraTM 40 to estimate particle morphology and, then, by using a laser granulometer Fritsch Analysette 22 Compact to determine the size distribution, adopting a volumetric assumption. As shown in Fig. 1a the mixed powder consists of mostly spherical particles indicating that the mixing has not damaged the starting particles. A consistent fraction of fine particles of a size below 5 µm tend to adhere to the coarsest ones resulting in the formation of large clusters of about 20 - 30 µm. Some Cu particles with varied sizes can be clearly observed among AlSi10Mg particles, indicated by white arrows in Fig. 1a. Particle diameters corresponding to 10% (d_{10}), 50% (d_{50}) and 90% (d_{90}) of the cumulative size distribution are 13.32, 28.22 and 44.77 µm, respectively (Fig. 1b). Considering these results and previous studies on aluminium alloys [16,25], it can be fixed a value of 30 µm for the layer thickness during the process.

Table 1 Chemical composition of the used powder (wt%); *the mixed one is calculated starting from the previous two compositions.

Alloy	Si	Fe	Cu	Mn	Mg	Ti	O	Al
AlSi10Mg	9-11	≤ 0.55	≤ 0.05	≤ 0.45	0.2-0.45	≤ 0.15	-	Bal.
HCP Cu	-	-	≥ 99.96	-	-	-	≤ 0.04	-
AlSi10Mg+4Cu*	8.6-10.6	≤ 0.55	4	≤ 0.45	0.19-0.43	≤ 0.15	≤ 0.04	Bal.

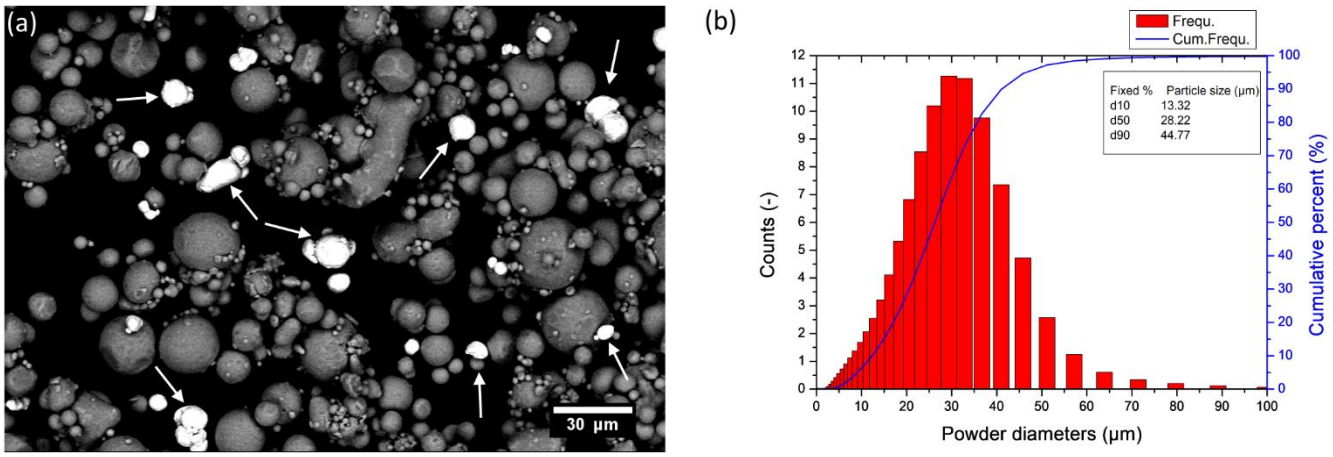

Fig. 1 (a) The AlSi10Mg+4Cu mixed powder observed by FESEM in BSE mode and (b) its particle size distribution with volumetric assumption.

2.2 Single Scan Tracks (SSTs) method, preparation and characterization

SSTs of Cu-AlSi10Mg mixed alloy were built by an EOSINT M270 Dual mode system (EOS Gmbh). In this system, a Yb-fiber laser is used to locally melt a thin powder layer with a wavelength of 1070 nm, a continuous power up to 200 W, a spot of 100 µm and a scanning speed up to 7000 mm/s. The building chamber provides a closed environment filled by argon as a protective gas. To reduce the thermal stresses between substrate and deposited tracks, the building platform was preheated at 100 °C. A modified building platform with removable discs of cast AlSi10Mg and of 40 mm diameter was adopted in the production of SSTs according to the system proposed by Aversa et al. [25]. The chemical composition of the disc was intentionally chosen as close as possible to the deposited alloy in order to prevent any contamination in the molten pool composition after the laser melting. To prepare the SSTs, a single powder layer of 50 µm thickness was accurately deposited using a self-developed recoating system only on the discs. This value was selected considering the real layer thickness obtained using a 30 µm as building platform displacement. The length of each scan track was 9 mm for all the experiments.

Two set of SSTs were built in two jobs with the process parameters summarized in Table 2.

A 5×5 matrix of *P* × *v* for a total of 25 combinations was used for the first job. Wide *P* - *v* ranges were specifically chosen for the purpose of verifying quickly the alloy processability and gaining preliminary insights on the corresponding operating window. To investigate the stability of the produced SSTs, on-top analysis was firstly carried out on SSTs surfaces by means of an optical microscope (OM) LEICA DMI 5000 M. Then, samples for melt pool (MP) characterization of SSTs were cut from the discs using a diamond saw, mounted in a thermosetting resin, polished by standard metallographic technique up to 1 µm and finally observed by OM. MP sections were taken in the middle of the scan track to ensure a reliable shape not affected by border instabilities [28]. The geometrical features of the investigated MP, i.e. width (*w*), total height (*h*), growth (*g*) and penetration in the substrate (*d*) as schematized in Fig. A 1, were evaluated by post-processing the corresponding MP micrographs via image analysis software ImageJ. Two main MP shape indicators were derived from this analysis: the total height to width ratio (*h/w*) and the growth to depth ratio (*g/d*).

Once the promising operating window was identified according to the former analysis, a narrow 3×4 matrix with *P* - *v* step size of 10 W and 100 mm/s, respectively, was selected around the optimum building parameters. In this way, 12 combinations were used in the second job. To check the continuity and uniformity of SSTs and to validate the final operating window, a detailed on-top investigation was performed on SSTs surfaces by using a Scanning Electron Microscope SEM PHENOM XL. To investigate the whole SST length, 5 micrographs were acquired for each SST. Furthermore, a comprehensive analysis of SSTs width (*w*) was automatically conducted through ImageJ. On each laser track 250 values of width were acquired. The mean width value ($\overline{w}$) of all SSTs was determined and used as a starting point in the definition of the hatching distance (h_d) for the production of massive samples, as described above.

Table 2 Laser power and scan speed values adopted for the SSTs analyzed to obtain the operating window parameters for AlSi10Mg+4Cu alloy.

Job	Goal	*P* × *v* matrix	*P* [W]	*v* [mm/s]
n°1	- To verify the alloy processability - To identify the operating windows	5×5	100, 130, 160, 180, 195	300, 600, 800, 1200, 1500
n°2	- To validate the selected operating windows - To determine h_d for massive samples	3×4	160, 170, 180	700, 800, 900, 1000

2.3 Design criteria, production, and characterization of massive samples

Table 3 summarizes the range of the key process parameters adopted in the production of parallelepipeds with dimensions of 10 mm × 10 mm × 5 mm. Samples were produced by using a layer thickness of 30 µm. The building platform was preheated at 100 °C. As reported by Calignano et al. [16], with the LPBF system adopted in the present study, many scanning strategies could be adopted. For the first job, it was decided to employ the unidirectional scanning strategy, to clearly understand the effect of the variations of laser power, scanning speed and hatching distance on porosity content and on the overlapping of SSTs. Moreover, a full factorial design of experiment (DOE) based on 2 factors (*P* and h_d) with 3 levels and 1 factor (*v*) with 4 levels was chosen for a total of 36 combinations.

Trying to identify the h_d values for Table 3, the focus was put on the overlapping of parallel scan tracks lines. It was decided to adopt Eq. 1, already used by Nie et. al [20]. In this way, by using the mean width value $\overline{w}$ of all the SSTs, it was possible to achieve different overlapping grade (φ), between nearby single tracks, namely completely overlapped, partially overlapped and not-overlapped tracks.

$$\varphi = \frac{w - h_d}{w} \cdot 100 \quad (1)$$

To determine the density of the manufactured parallelepipeds, as-built samples were detached from the building platform using an electrical discharge machining (EDM) system. The samples outer surface was removed by grinding with SiC abrasive papers. Afterward, the density was evaluated in accordance with the Archimede's principle by

using a Sartorius density measuring set YDK 01 [29], with 3 measurements for each sample. As theoretical density of the AlSi10Mg+4Cu alloy, a value of 2.74 Kg/dm^3 was estimated by using the volumetric rule of mixtures (ROM) [30].

All the data collected from the first job were analyzed using the statistical analysis software Minitab 17. Global analysis of variance (ANOVA) was applied to investigate parameters with significant effects on porosity. A significance level (*p-value*) less than 0.005 was chosen. In addition, a cross-section along the building direction and perpendicular to the laser scan tracks for each specimen was polished down to 1 µm and investigated by OM to examine the presence of internal defects, e.g. pores, un-melted powder particles, and eventually cracks. The aim of these analyses was the determination of parameters that need to be discarded for further experiments.

Then, a second job adopting a rotated scanning strategy was planned. As reported in a previous study by Manfredi et al., this leads to isotropic properties in the plane parallel to the building platform [31]. In this case, a full factorial DOE with a restricted operating window based on 2 factors (*P* and h_d) with 2 levels and 1 factor (*v*) with 4 levels was designed. Again, all the samples were subjected to Archimede's density analysis in order to evaluate the porosity content. Hence, on the polished surface of specimens with porosity lower than 1.5%, Brinell hardness (HB10) was evaluated applying a load of 62.5 Kg using an hardness tester EMCO TEST M4U 025. On each sample ,5 measurements were performed according to ASTM E10-18 [32], in order to have a preliminary insight on the mechanical properties of the obtained AlSi10Mg+4Cu parallelepipeds.

Table 3 The range of factors and levels used for the DOE of the two jobs to manufacture parallelepiped samples.

Job	Scanning strategy	$P \times v \times h_d$ matrix	*P* [W]	*v* [mm/s]	h_d [mm]
n°1	Unidirectional, 0°	3×4×3	160, 170, 180	700, 800, 900, 1000	0.08, 0.12, 0.14
n°2	Rotated, 67°	2×4×2	170, 180	700, 800, 900, 1000	0.12, 0.14

3. Results

3.1 Single Scan Tracks

Fig. 2a shows the top surfaces of SSTs produced according to a 5×5 *P-v* matrix (see Table 2). Over the entire range of parameters, two types of scan tracks can be recognized:

I) Unstable SSTs. At low laser powers, SSTs result to a large extent in irregular surfaces. Under the lowest scanning speed, the applied laser energy is sufficient to melt the powder to a significant extent, but top-surfaces exhibit spiked traces of partially melted material along the sides, as shown in Fig. A 2. As the scanning speed is increased, tracks show a tendency to be more discontinuous and a preliminary balling phenomenon arises. Here, pronounced bulged balls followed by tight necking areas are clearly visible on SSTs surfaces. Finally, at 1500 mm/s and 100 W, the laser track splits into separated drops, caused by the limited amount of liquid formed because the energy of laser input decreases.

II) Stable SSTs. At high laser powers, with the whole range of applied scanning speeds, a sufficient amount of liquid formed and yielded continuous and regular molten cylinders, free of pronounced balls.

Even though some tracks classified as stable show minor defects, e.g. a slightly marked hump effect at 180 W - 800 mm/s and a wide heat affected zone at 195 W - 300 mm/s, they could be considered acceptable at this stage since this on-top analysis is intended as an early basic fast screening to verify solely the presence of macro-defects on SSTs surfaces. For this reason, a detailed investigation on MP cross-sections was carried out with the purpose to add more information to the former analysis and to determine the processing map.

Fig. 2b visually emphasizes shape differences among the investigated MPs, while

Table A ***1*** summarizes the dimensions of the geometrical features of MPs. As can be observed in Fig. 2b, MPs can be classified as irregular and regular:

I) Irregular MPs. When the applied power is relatively low at scanning speeds lower than 1200 mm/s, the laser energy is insufficient to fully melt the underlying substrate and, as a result, shallow MPs with bumpy shape were generated. In these cases, MPs are characterized by a *h/w* ratio ≥ 0.63, which means that the shape is close to spherical. Furthermore, these MPs have both significantly asymmetrical position on the substrate, with a *g/d* ratio ≥ 1.47, together with a poor penetration. On the other hand, under the highest scanning speed, i.e. 1500 mm/s, and power values lower than 160 W, the laser radiation interacts with the

powder bed for a short time resulting in splashed MPs with extremely low growth. In addition, also using a constant laser power of 195 W, at both the lowest and highest speeds, irregular melt pools occur: in the first case, a deep and convex shaped MP with a markedly high *d* value appears, which means that a huge amount of energy density is applied; in the second case, the MP shape is more spherical with a reduced penetration, as a consequence of a shorter laser-material interaction.

II) Regular MPs. As highlighted in Fig. 2b, by using power values ranging from 160 to 195 W, quite regular MPs are formed. It is evident from the results that all such MPs develop quasi-elliptical profiles, having a *h/w* ratio between 0.39 and 0.62. Among these, two MPs with the optimum shape are identified (see the green box in Fig. 2b). In fact, when the applied laser power is 160 or 180 W, at a scanning speed of 800 mm/s, symmetrical MPs with *g/d* ratio, respectively equal to 1.06 and 1.14, were produced. Furthermore, they are found to be sufficiently deep to mix strongly with the substrate below whilst avoiding excessive re-melting.

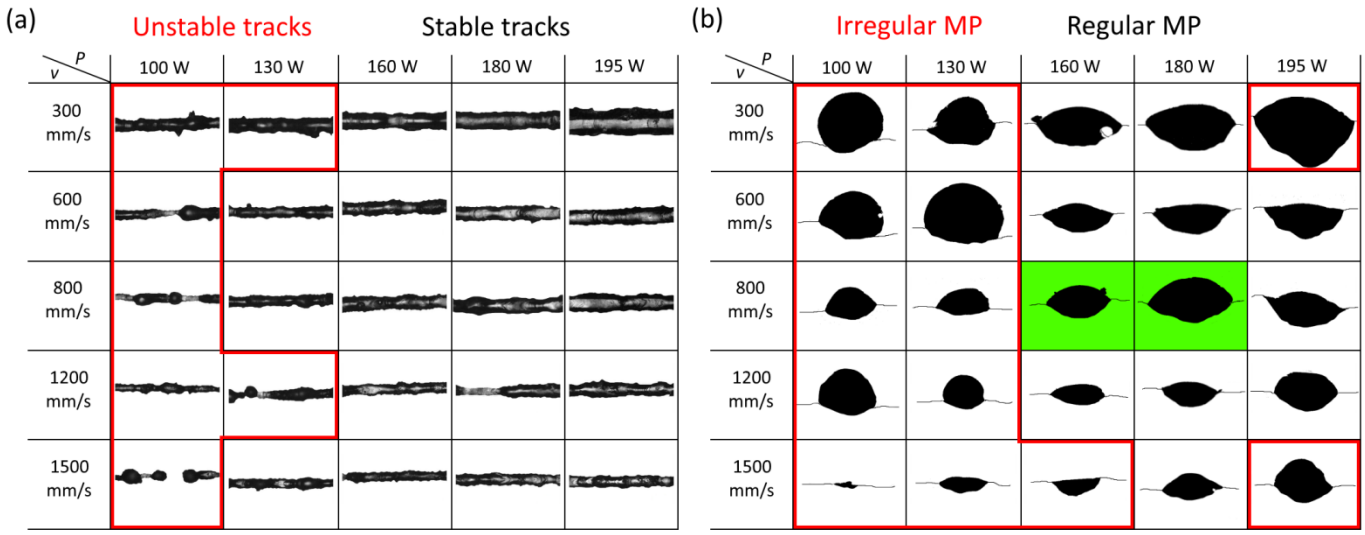

Fig. 2 (a) On-top surfaces of SSTs and (b) MP cross-sections according to the 5×5 *P-v* matrix.

As a result of the first SSTs job, the processing map of Fig. 3 was obtained, in which three different scenarios could be identified. Firstly, the Unstable SSTs - Irregular MPs scenario arises, where the laser energy is not efficiently absorbed by the powder, creating laser tracks with visible defects and MPs with a pronounced asymmetry on the substrate. Accordingly, these building parameters are excluded for further trials. Secondly, stable SSTs with irregular MPs are obtained at certain values of power and speed, corresponding to the yellow regions in Fig. 3. Here, the applied energy is sufficient to preserve the scan track continuity, but shallow, splashed or convex MPs, not appropriated for a part production, are formed. Finally, the Stable SSTs - Regular MPs scenario corresponds to the promising operating window for the investigated alloy.

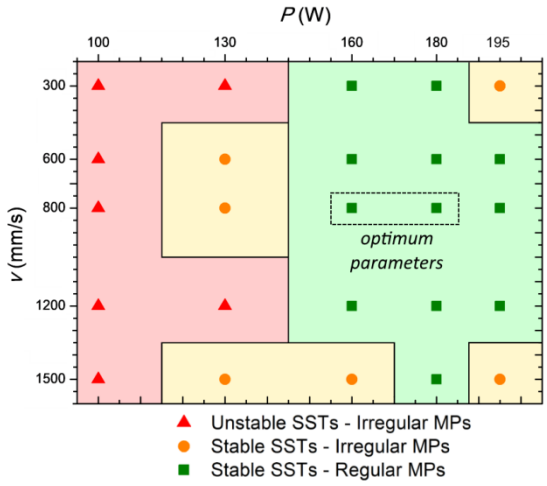

Fig. 3 Processing map of the AlSi10Mg+4Cu alloy for the estimation of building process parameters effects.

Therefore, the operating window is considered as a specific region of the processing map where a proper

combination of power and speed generates continuous SSTs and stable MPs with quasi-elliptical shape. Within this scenario, *P*-*v* couples with values of 160 W-800 mm/s and 180 W- 800 mm/s (see the dotted line in Fig. 3), allow to obtain the optimum MPs shapes combined with stable tracks. Hence, these *P*-*v* couples were fixed as a starting point in designing the second SSTs job (see Table 2) and, accordingly, a restricted 3*P* × 4*v* operating window was built around these parameters.

In the second job, SSTs were produced with the purpose to fine tune the process parameters for an operating window.

Fig. 4a illustrates SEM micrographs of the second job SSTs surfaces. As expected, macro-defects, such as ripples, distortions, and droplets, are not present at this stage. All the investigated SSTs show an appreciable continuity, validating the reliability of the selected operating window. Nevertheless, varied types of scan track morphologies can be observed. On one hand, under medium-low *P* values within the whole range of used scanning speeds, laser tracks are relatively smooth and linear. Only a few partially melted powder particles and laser-induced melt splashes can be observed at 160 W-800 mm/s and 170 W-700 mm/s, respectively. On the other hand, by increasing the laser power to 180 W, the SSTs continuity is well preserved, but SSTs exhibit parts with a pronounced bulging surface. In agreement with literature, this occurs especially when the linear energy density increases and, therefore, the melt pool viscosity decreases [33].

Width values of SSTs were also determined at this stage. As can be seen from Fig. 4b, for a given scanning speed value the track width has a linear dependence on the applied power. Actually, *w* values increase as the power is increased. On the basis of the micrographs of Fig. 4a, the mean width value $\overline{w}$ of all SSTs tracks was determined as 131 µm.

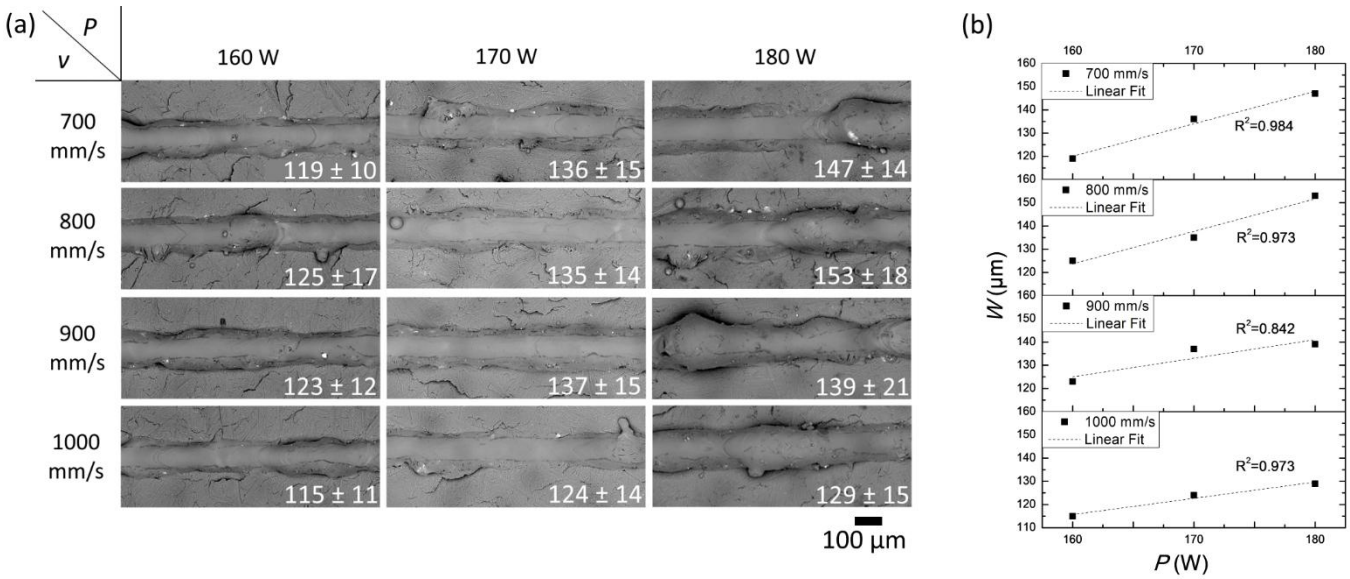

Fig. 4 (a) SEM micrographs of SSTs surfaces according to the 3×4 *P*-*v* matrix, used in the optimized SSTs job. Width (*w*) values of single tracks are summarized on the bottom-right side of each *P*-*v* box. (b) Significant relationships between SSTs width and laser power.

3.2 Parallelepiped massive samples

The mean width value $\overline{w}$ of the second job SSTs was used as reference to determine the h_d values for massive samples production with unidirectional scanning strategy. The results of density analysis for these samples are summarized in Table A 2. Quite high values between 95.66 and 99.30 % are obtained. In Table A 3, the analysis of variance on porosity content is summarized. The building parameters with *p*-value less than 0.005 are labelled as significant. In this regard, ANOVA results reveal that the influence of power and hatching distance on the amount of porosity is highly significant, as they show very low *p*-values. Both of these effects can be clearly appreciated by observing the main interaction plots reported in Fig. 5.

In fact, considering Fig. 5a, it is possible to notice an increase in porosity by increasing *v*. The porosity values of samples obtained at 160 W are always the highest and they decrease as the applied *P* increases, regardless of the applied scanning speed.

Observing the interaction between *P* and h_d in Fig. 5b, it could be observed that by using an h_d of 0.08 mm, the highest porosity values are obtained in each *P* series. On the other hand, when h_d increases, an appreciable

reduction in porosity is achieved ranging from 0.08 to 0.12 mm of h_d and then, by further increasing h_d to 0.14 mm, very slight variations in porosity are found.

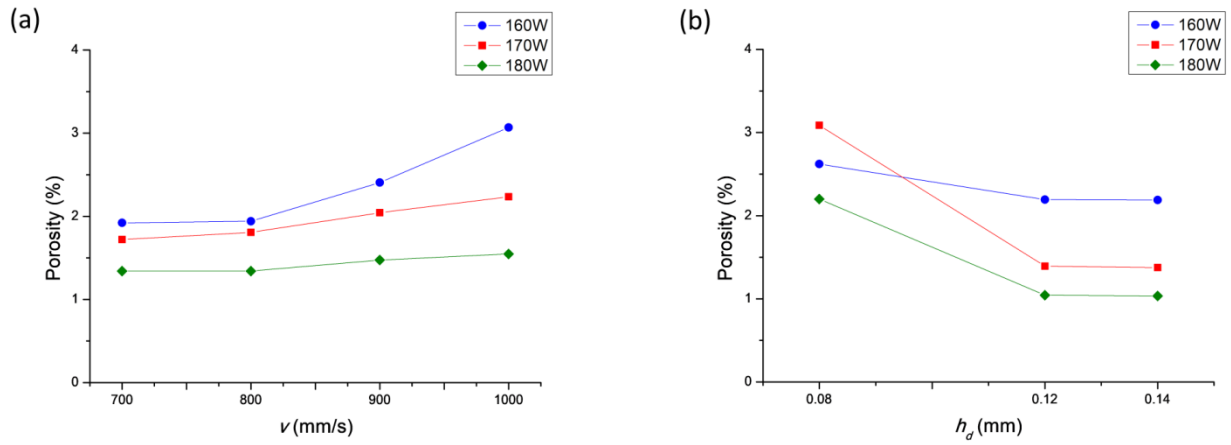

Fig. 5 Main interaction plots for porosity. (a) Relationship between porosity and scanning speed at varied power levels; (b) porosity values vs. hatching distance according to the used power.

Fig. 6 shows the porosity values as a function of the SSTs overlap φ at different applied power levels. φ values were defined according to Eq. 1 by using the mean width value w of each SST, determined by image analysis in the second SSTs job, as stated before.

Therefore three scenarios between nearby single tracks, corresponding to not-overlapped ($\varphi < 0\ \%$), partially overlapped ($0\ \% \leq \varphi \leq 20\ \%$) and completely overlapped ($\varphi > 20\ \%$) tracks, were superimposed on Fig. 6.

As easily observable from the graph, samples with lower porosity completely fall within the partially overlapped scenario. Actually, it can be noted that a mild reduction in porosity is generally achieved moving from the not-overlapped to the partially overlapped scenario and, then, a marked increment is observed by further increasing φ to the completely overlapped zone.

Considering these results, it can be stated that a partial overlap ($0\ \% \leq \varphi \leq 20\ \%$) between neighbouring scan tracks is the most desirable condition to produce dense massive samples. In fact, it is supposed that when the not-overlapped scenario is reached, aligned process porosities might arise as a consequence of farther SSTs. On the other hand, when the completely overlapped scenario is reached, an excessive laser re-melting could generate unstable melt pool and the subsequent formation of irregular porosities.

These remarks can be explained in detail by considering both the iso-power (dotted lines) and iso-hatching (dashed lines) behaviors in Fig. 6 and the polished cross-sections in Fig. 7 of samples built at 900 mm/s.

As can be seen from the iso-power behavior, porosity reaches the minimum in the partially overlapped scenario for all *P* series (see a^{ii}, b^{ii} and c^{ii}). Furthermore, in line to what has been suggested so far, when a quite negative φ value occurs, columnar and elongated process porosities are identifiable on polished cross-section of a^{i} in Fig. 7 Additionally, irregular shaped porosities can be observed in Fig. 7 on all surfaces of a^{iii}, b^{iii} and c^{iii} built at higher φ value. The presence of such porosities could be explained by the fact that, where φ is large, the laser beam overly remelts the track previously produced. Thus, this generates an excessive size distortion of the melt pool, changing its shape from regular to irregular.

Considering the iso-hatching behaviors, it can be pointed out that φ increases as the applied *P* increases. Interestingly, the observed behaviour can be correlated with the linear relationship between w and *P* provided in Fig. 4b. Actually, by keeping constant h_d and increasing *P*, the width w linearly increases with *P* and, as a consequence, the extent of overlap φ also increases.

This increment of φ was found beneficial in term of porosity when the iso-hatching behaviour at 0.14 mm is considered. In fact, increasing *P* and, consequently, increasing φ, porosity values are reduced from 2.22 % of a^{i} to 1.13 % of c^{i}. The main reason behind this reduction in porosity could be that higher *P* (180 W) enables to work using φ very near to the partially overlapped scenario, which seems to be the appropriate arrangement of SSTs.

Considering the iso-hatching behaviour at 0.12 mm, a medium-low level of porosity (below 1.50 %) is obtained as the φ values of a^{ii}, b^{ii} and c^{ii} are in the partially overlapped range. On the other hand, when the iso-hatching at 0.08 is considered, a quite high amount of large porosities appears since it is being worked far away from the desirable overlap condition.

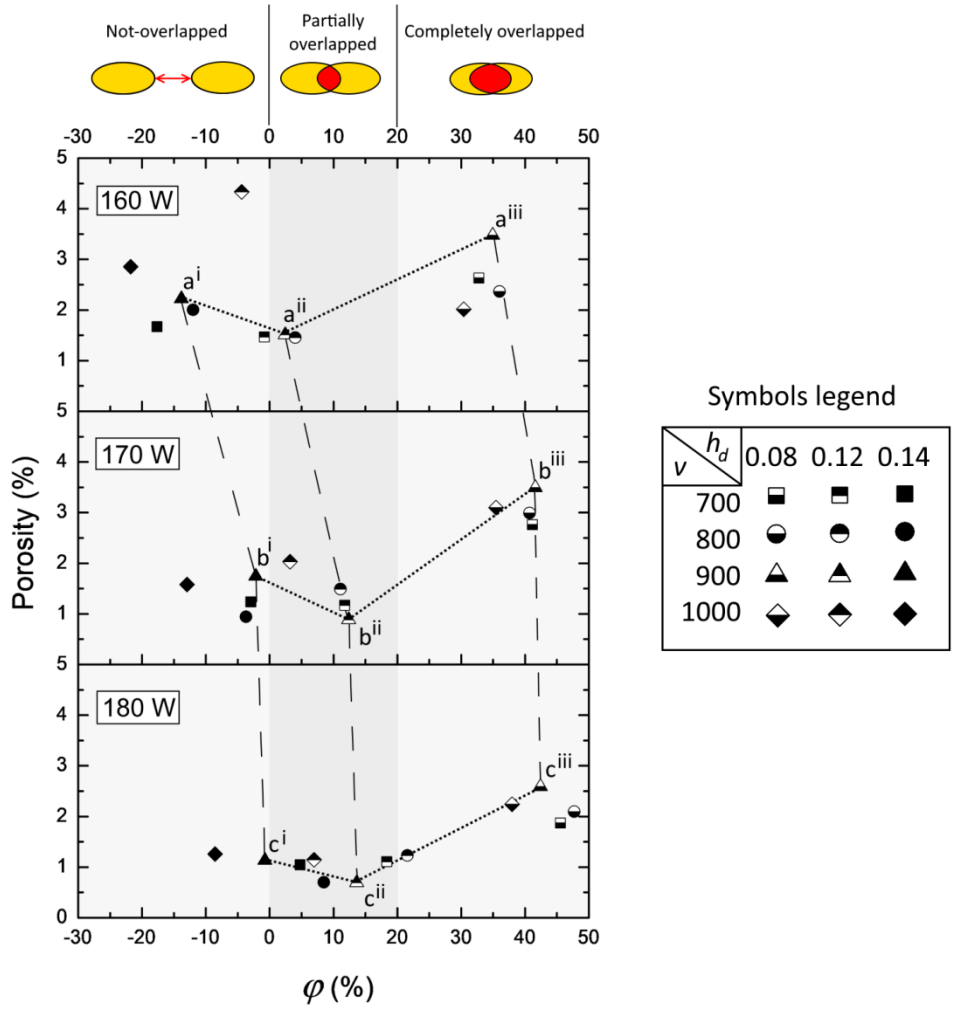

Fig. 6 Effect of φ on porosity values. Dotted and dashed lines refer respectively to the iso-power and iso-hatching behaviours at 900 mm/s.

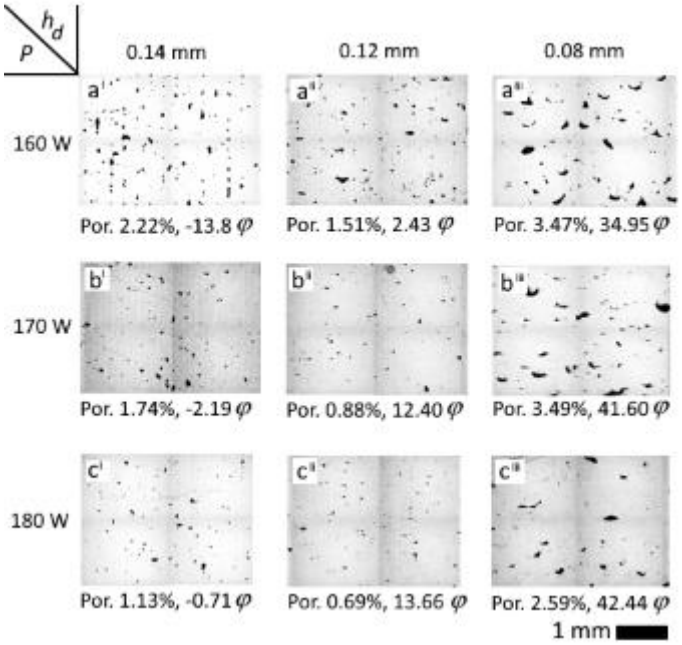

Fig. 7 Cross-sections of as-built samples with unidirectional scanning strategy at 900 mm/s, according to the 3×3 *P*-h_d matrix. The label on the top-left of each *P*-h_d box refers to the labelled points showed in Fig. 6.

On the basis of the previous results, *P* and h_d values of 160 W and 0.08 mm, respectively, are excluded for the second job to manufacture parallelepiped samples as they imply porosity values higher than 1.50 % (see Table A 4).

Table A 5 summarizes density results for the second job: significantly high values are obtained, which vary in a narrow range, i.e. from 98.62 to 99.16 %.

The results of porosity of these massive samples are plotted as a function of the applied scanning speed in Fig. 8. This suggests that in this process window the effect of *v* on porosity is negligible. Similarly, also the influence of *P* and h_d is not completely clear as the variation between porosity values is extremely low.

Therefore, it is thought that the combinations of *P*, *v* and h_d used for the second job can all be adopted in manufacturing AlSi10Mg+4Cu parts.

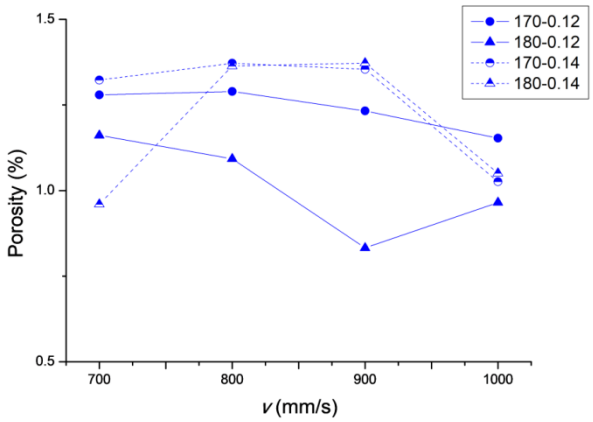

Fig. 8 Variation of porosity with the applied scanning speeds for the second job of parallelepiped AlSi10Mg+4Cu samples.

Finally, HB10 tests were performed to have the first insights about hardness of the samples. Furthermore, in view of an industrial application, also the productivity was considered and, accordingly, the build-up rates for the optimized process parameters were estimated.

HB10 mean values listed in Table A 5, indicate that the slight addition of Cu (4 wt%) to AlSi10Mg alloy provides a significant increase in hardness. In comparison to the HB10 value of the as-built AlSi10Mg, which is found to be 129 HB [34], an increment between 6.5 and 16% was recorded. This hardness variation cannot be explained by the different porosity levels of samples because porosity is found to vary in a restricted range (see Fig. 8). Conversely, it is more reasonable to ascribe the hardness variation to the in-situ AlSi10Mg+4Cu alloying, to the subsequent Cu mixing in Al and to the formation of Al(Cu) solid solution. In this context, an EDS analysis map reported in Fig. 9b demonstrates that Cu spread within the Al matrix. Nevertheless, further work is planned in order to identify the presence of possible Al-Cu intermetallic precipitates inside the Al matrix, as recently investigated by Wang et al [35].

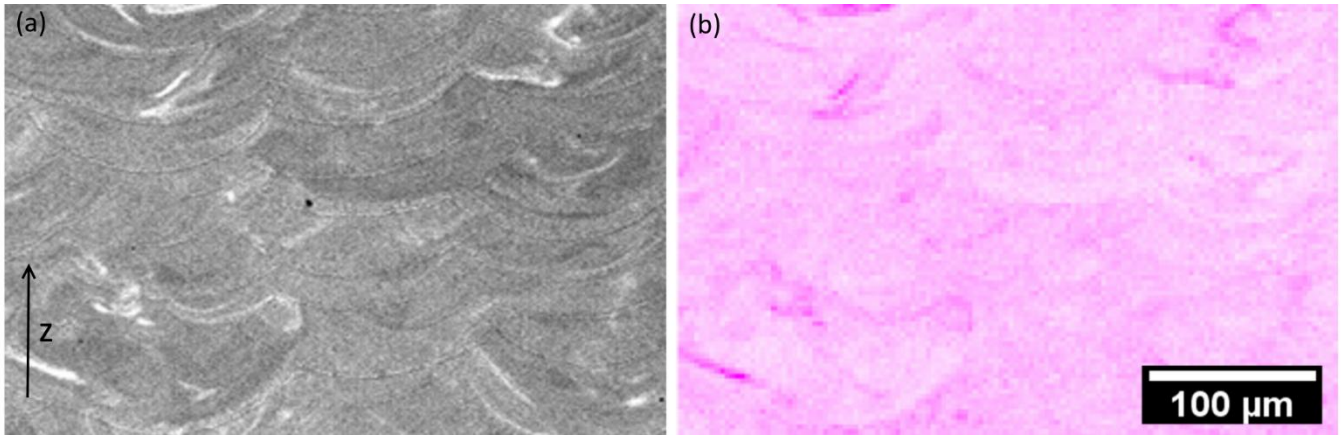

Fig. 9 EDS analysis performed on as-built massive sample surface along the building direction. (a) SEM micrograph of a polished cross-section; (b) map of the Cu distribution.

Fig. 10 shows the relationships among hardness (*HB10*), volumetric energy density (*VED*) and build-up rate ($\dot{V}$), determined according to Eq. 2 and Eq. 3, respectively [36,37]:

$$VED = \frac{P}{v \cdot h_d \cdot t} \quad \left[\frac{J}{mm^3}\right] \tag{2}$$

$$\dot{V} = v \cdot h_d \cdot t \quad \left[\frac{cm^3}{h}\right] \tag{3}$$

where t is the layer thickness fixed at 0.03 mm in this study. The obtained data are reported in Table A 5.

In Fig. 10, a general reduction of hardness on growing VED is evident. Concerning the build-up rate, one may postulate that the higher the VED, the lower the build-up rate.

Considering both the hardness and build-up rate behaviour as a function of VED, 3 operating range conditions can be identified in Fig. 10. First, when relatively low VED values are applied and, as a consequence, significantly high $\dot{V}$ are accomplished (≥ 12.96 cm^3/h), medium-high HB10 values are achieved. On the contrary, under higher VED the process results in slightly low productivity rates, i.e. $\dot{V}$ ≤ 10.58 cm^3/h, and medium-low hardness values. Finally, as far as the intermediate VED is concerned, i.e. between 50 and 60 J/mm^3, an appreciable productivity $\dot{V}$ is obtained with HB10 varying from very low to quite high values.

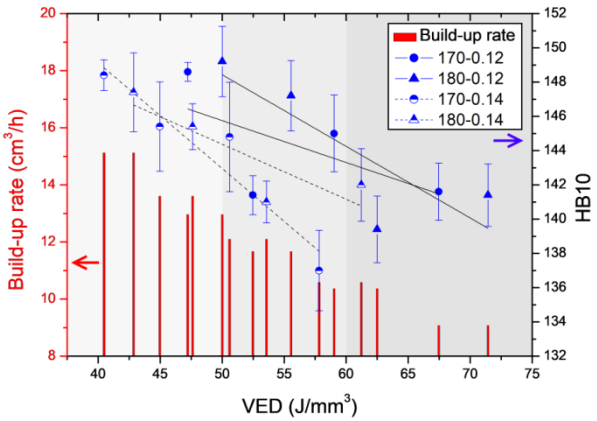

Fig. 10 Significant relationships between hardness, build-up rate and VED for the AlSi10Mg+4Cu massive samples of the second job.

In conclusion, when high productivity is needed, lower VED should be adopted and, accordingly, as-built parts with medium-high hardness are obtained. Nevertheless, it should be considered that by using high scanning speed, a high internal residual stresses occurs and, then, an annealing treatment must be performed in the post-processing operations, increasing the production cost [13,38]. Furthermore, one may also consider that high scan speed could negatively affect the surface roughness [33]. On the other hand, when there is high demand in top surface quality, higher VED should be used. As a consequence, lower productivity rates and medium-low hardness are achieved.

Hence, on the basis of the results showed in Fig. 10, it is possible to select the proper main process parameters (*P*, *v*, h_d) according to both the final part application and industrial needs, like productivity.

4. Discussion

SSTs were at first produced by using a large *P* × *v* matrix in order to verify quickly the alloy processability in dependence of both laser power and scanning speed [39]. To do this, on-top and cross-section analyses of SSTs were used to define a promising processing window in line with earlier works in literature [23–26, 40–42]. In this way it was possible to determine a reliable processing map for the studied alloy, which is characterized by stable SSTs and regular MPs (see Fig. 3). Moreover, the small quantity of mixed powder required in the SSTs production coupled with the simple and fast characterization (see Section 2.2) are added values to such approach. Hence, from merely one SSTs production, it has been shown that it is possible to gain important details on the alloy processability without wasting materials and time, which are cost-effective aspects to be considered in the development of new alloy for LPBF part manufacturing [13].

At that point, once the best *P*-*v* couples were identified, an additional job of SSTs was performed around these values to finely tune the process parameters. Then, SSTs widths were evaluated in order to determine h_d values for the production of parallelepiped massive samples. At this stage, the unidirectional scanning strategy was used to clearly understand the effect of *P*, *v* and h_d on porosity and on the SSTs overlap φ. Considering all of the experimental data mentioned so far, results of porosity as a function of φ shown in Fig. 6 seems to be promising. Actually, there is evidence to suggest that a partially overlapping grade φ between neighbouring tracks can minimize the presence of porosity at each level of *P* for the selected operating window. On the contrary, when φ comes out of this range, porosity increases due to an undesirable SSTs arrangement (see Fig. 7). This experimental finding can be adopted as a useful criterion in the process parameters optimization route. In fact, according to the determined SST

width, which is controlled by *P* and *v*, it can be possible to select a-priori only one h_d value so as to assure the partially overlapped scenario ($0\ \% \leq \varphi \leq 20\ \%$) and, as a consequence, to increase the density of massive samples. This overlapping criterion is the reverse function of Eq. 1 and is summarized for clarity in Eq. 4:

$$h_d = w \cdot \left(1 - \frac{\varphi}{100}\right) \tag{4}$$

where *w* is the measured SSTs width and φ is the overlap value ranging between 0 and 20 %.

Moreover, it is thought that this innovative methodology enables to exploit only single scan tracks to define process parameters (*P*, *v* and also h_d) for LPBF massive samples production, minimizing the number of the samples produced and accelerating the optimization process. It could also represent the indispensable link between the characteristics of one single track and the corresponding parallelepiped sample of the same material.

To validate this novel methodology, the values of *P*, *v* and h_d adopted in previous studies for the EOS M270 Dual Mode machine and AlSi10Mg powders were considered [31,43]. Hence, a single scan track of AlSi10Mg was produced at 195 W and 800 mm/s with the procedure explained in Section 2.2. Then, SST mean width w was determined and its value was found to be 170 ± 14 µm. Interestingly, by inserting the determined SST w and the h_d previously adopted (0.17 mm) in Eq. 1, a φ value of 0 % was found, which means theoretically adjacent scan tracks and, accordingly, high density level. This is consistent with the work carried out in this study.

By applying a posteriori this novel methodology to our research, from results summarized in Table A 4, it can be concluded that the h_d of 0.12 mm allows to work in the partially overlapped scenario for most of the considered *P*-*v* couples. Thus, once the best *P*-*v* combinations (see Fig. 4) and the proper h_d are determined through the SSTs analysis, according to this novel approach only 12 ($3P \times 4v \times 1h_d$) combinations of parallelepiped massive samples with a rotated scanning strategy should be directly produced, saving time-intensive DOE experiments. Then, the optimal process parameters for parts production could be selected according to density, mechanical properties (at the present stage, hardness) and productivity.

Conclusions

The present work intends to propose a novel method to process new alloy compositions by LPBF process. Specifically, a new AlSi10Mg+4Cu alloy was prepared by simple mixing of powders and processed through LBPF to produce Single Scan Tracks (SSTs) and massive parallelepiped samples. The main findings of this study can be summarized as follows:

1) a reliable operating window, which is characterized by stable SSTs and regular MPs, is determined by quickly analysing SSTs on-top and cross-section surfaces;
2) ANOVA analysis performed on porosity results of parallelepiped massive samples produced using the unidirectional scanning strategy shows that *P* and h_d are the main significant parameters to be considered within the selected operating window;
3) a partially overlapping grade φ in the range of 0 - 20% can minimize the porosity content at each level of used *P*, demonstrating that a proper overlap between nearby SSTs, and therefore a specific h_d, is fundamental to achieve high level of density;
4) AlSi10Mg+4Cu samples produced using the optimum process parameters and the rotating scanning strategy showed density levels up to 99.16 %;
5) In terms of mechanical properties, Cu addition to AlSi10Mg alloy provides an increment of hardness between 6.5 and 16%, depending on the applied VED;
6) the overlapping criterion is validated considering the parameters for the EOS M270 Dual mode machine and AlSi10Mg powders used in previous studies.

Therefore it was demonstrated how near fully dense samples made of a new alloy can be obtained through an accelerated definition of the main LPBF process parameters, which involves few steps. At first, a *P*-*v* operating window is easily defined by means of the SSTs approach saving time and starting powders. Then, the proper h_d is designed according to the proposed overlapping criterion and massive samples can be directly produced by using the best *P*-*v* combinations, the designed h_d and the desired scanning strategy, avoiding many time-consuming DOE experiments. At the end, the process parameters for the new alloy can be defined according to the promising compromise between part properties and industrial needs.

Acknowledgments

The authors would like to acknowledge the regional project STAMP (Sviluppo Tecnologico dell'Additive Manufacturing in Piemonte).

Appendix

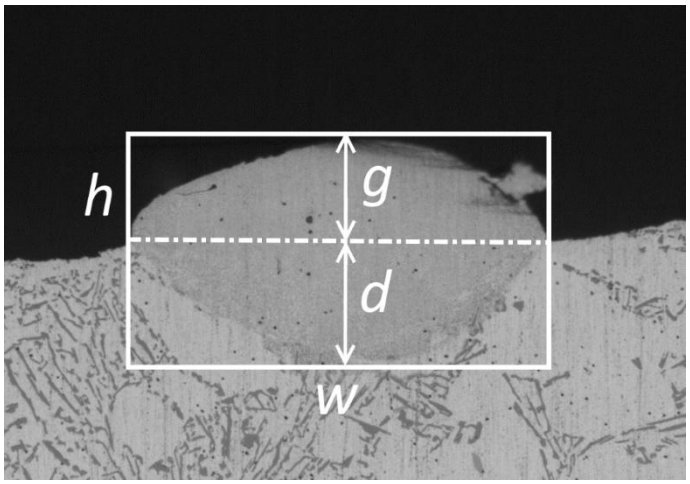

Fig. A 1 Scheme of the MP cross-section with the dimensions used to determine the MP geometrical features. The investigated MP geometrical features are width (*w*), total height (*h*), growth (*g*) and penetration in the substrate (*d*). The obtained aspect-ratio indicators are the height to width ratio (*h/w*) and the growth to depth ratio (*g/w*).

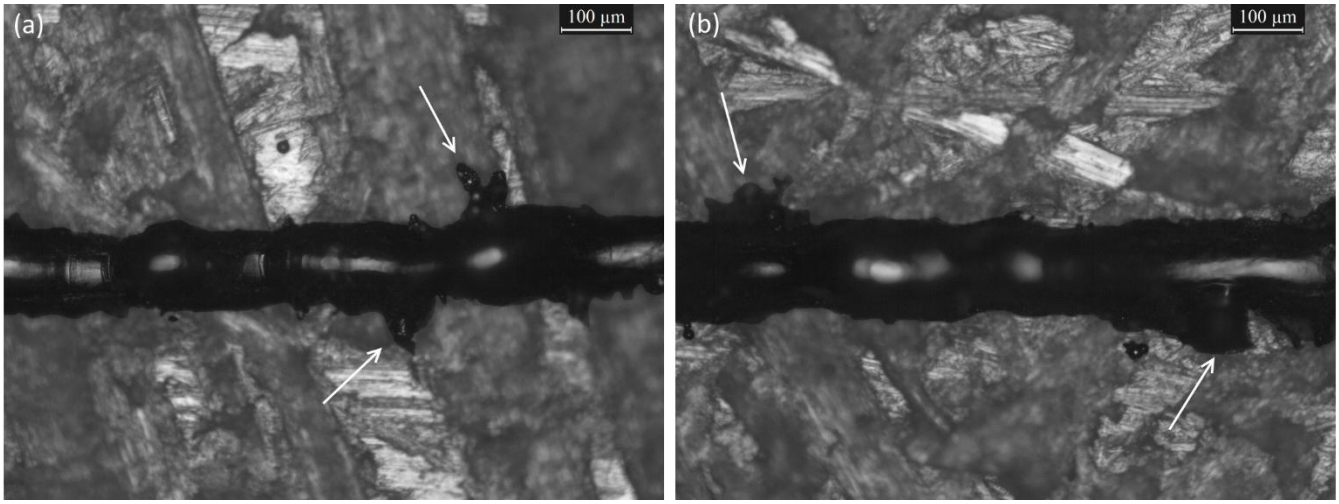

Fig. A 2 On-top surfaces of AlSi10Mg+4Cu SSTs built with (a) 100 W and (b) 130 W at a constant scanning speed of 300 mm/s. White arrows indicates traces of incongruently melted material along the tracks side.

Table A 1 Results of the quantitative analysis on MP cross-sections. Geometrical characteristics are determined according to Fig. A 1.

***P* [W]**	***v* [mm/sec]**	***LED* [J/mm]**	***w* [µm]**	***h* [µm]**	***h/w* [-]**	***g* [µm]**	***d* [µm]**	***g/d* [-]**
100	300	0.33	134	92.56	0.68	70.26	22.30	3.15
	600	0.16	120	90.96	0.74	64.45	26.51	2.43
	800	0.12	96	61.45	0.63	37.94	23.51	1.61
	1200	0.08	107	87.35	0.81	67.55	19.80	3.41
	1500	0.06	45	13.43	0.30	6.10	7.33	0.83
130	300	0.43	128	91.93	0.70	54.65	37.28	1.47
	600	0.21	148	113.44	0.76	84.23	29.21	2.88
	800	0.16	101	50.33	0.49	37.09	13.24	2.80
	1200	0.10	78	63.29	0.82	47.29	16	2.96
	1500	0.08	91	31.12	0.34	12.21	18.91	0.65
160	300	0.53	169	74.28	0.44	33.52	40.76	0.82
	600	0.26	132	55.02	0.41	21.50	33.52	0.64

	800	0.2	120	62.36	0.51	32.12	30.24	1.06
	1200	0.13	95	54.75	0.57	29.77	24.98	1.19
	1500	0.10	91	36.02	0.39	8.18	27.84	0.29
180	300	0.6	168	88.1	0.52	39.72	48.38	0.82
	600	0.3	145	57.08	0.39	13.05	44.03	0.30
	800	0.22	155	83.92	0.54	44.77	39.15	1.14
	1200	0.15	111	46.81	0.42	15.23	31.58	0.48
	1500	0.12	108	50.25	0.46	28.70	21.55	1.33
195	300	0.65	187	131.44	0.70	41.15	90.29	0.46
	600	0.32	148	67.14	0.45	13.90	53.24	0.26
	800	0.24	156	66.59	0.43	19.39	47.20	0.41
	1200	0.16	117	73.36	0.62	38.55	34.81	1.11
	1500	0.13	109	82.15	0.75	50.77	31.38	1.62

Table A 2 Results of density analysis for all the parameters considered in the DoE of AlSi10Mg+4Cu parallelepiped samples by LPBF with unidirectional scanning strategy.

Specimen	*P* [W]	*v* [mm/s]	h_d [mm]	$\rho_{Arch.}$ [Kg/dm^3]	$\rho_{Rel.}$ [%]	Porosity [%]
1	160	700	0.08	2.67	97.37	2.62
2	170	800	0.12	2.70	98.51	1.48
3	180	700	0.14	2.71	98.95	1.04
4	160	1000	0.08	2.68	97.98	2.01
5	170	1000	0.14	2.70	98.41	1.58
6	180	800	0.14	2.72	99.30	0.69
7	170	700	0.12	2.71	98.83	1.16
8	180	900	0.08	2.67	97.40	2.59
9	160	1000	0.14	2.66	97.14	2.85
10	160	900	0.08	2.64	96.52	3.47
11	160	800	0.14	2.68	97.99	2.00
12	170	700	0.14	2.71	98.76	1.23
13	170	700	0.08	2.66	97.24	2.75
14	180	700	0.12	2.71	98.89	1.10
15	170	1000	0.08	2.65	96.90	3.09
16	180	900	0.14	2.71	98.86	1.13
17	170	900	0.08	2.64	96.50	3.49
18	160	1000	0.12	2.62	95.66	4.33
19	180	700	0.08	2.69	98.12	1.87
20	170	900	0.12	2.71	99.11	0.88
21	180	1000	0.14	2.70	98.74	1.25
22	180	1000	0.08	2.68	97.75	2.24
23	180	900	0.12	2.72	99.30	0.69
24	160	900	0.14	2.68	97.77	2.22
25	180	800	0.12	2.71	98.77	1.22
26	160	800	0.08	2.67	97.63	2.36
27	170	800	0.08	2.66	97.00	2.99
28	180	1000	0.12	2.71	98.85	1.14
29	160	800	0.12	2.70	98.54	1.45
30	160	900	0.12	2.70	98.48	1.51
31	170	800	0.14	2.71	99.05	0.94
32	170	900	0.14	2.69	98.25	1.74
33	160	700	0.14	2.69	98.32	1.67
34	160	700	0.12	2.70	98.53	1.46
35	180	800	0.08	2.68	97.90	2.09
36	170	1000	0.12	2.68	97.97	2.02

Table A 3 Analysis of Variance (ANOVA) of the porosity content of AlSi10Mg+4Cu samples produced by LPBF using unidirectional scanning strategy.

Source	DF	Sum of squares	F-value	p-value	Statistical significance (p < 0.005)
P	2	4.990	9.73	0.003	Significant
v	3	2.267	2.95	0.076	Not significant
$\boldsymbol{h_d}$	2	9.647	18.82	0.000	Significant
$P \cdot v$	6	0.929	0.60	0.723	Not significant
$P \cdot \boldsymbol{h_d}$	4	2.172	2.12	0.141	Not significant
$v \cdot \boldsymbol{h_d}$	6	3.781	2.46	0.087	Not significant
Error	12	3.075			
Total	35	26.863			

Table A 4 Porosity values of AlSi10Mg+4Cu samples produced by LPBF using unidirectional scanning strategy as a function of varied overlap modes between SSTs.

P [W]	v [mm/s]	h_d [mm]	φ [%]	Porosity [%]	Overlap Scenario
160	700	0.08	32.77	2.62	Compl. φ
		0.12	-0.84	1.46	Not. φ
		0.14	-17.65	1.67	Not. φ
	800	0.08	36.00	2.36	Compl. φ
		0.12	4.00	1.45	Partial. φ
		0.14	-12.00	2.00	Not. φ
	900	0.08	34.96	3.47	Compl. φ
		0.12	2.44	1.51	Partial. φ
		0.14	-13.82	2.22	Not. φ
	1000	0.08	30.44	2.01	Compl. φ
		0.12	-4.35	4.33	Not. φ
		0.14	-21.74	2.85	Not. φ
170	700	0.08	41.18	2.76	Compl. φ
		0.12	11.77	1.16	Partial. φ
		0.14	-2.94	1.23	Not. φ
	800	0.08	40.74	2.99	Compl. φ
		0.12	11.11	1.48	Partial. φ
		0.14	-3.70	0.94	Not. φ
	900	0.08	41.61	3.49	Compl. φ
		0.12	12.41	0.88	Partial. φ
		0.14	-2.19	1.74	Not. φ
	1000	0.08	35.48	3.09	Compl. φ
		0.12	3.23	2.02	Partial. φ
		0.14	-12.90	1.58	Not. φ
180	700	0.08	45.58	1.87	Compl. φ
		0.12	18.37	1.10	Partial. φ
		0.14	4.76	1.04	Partial. φ
	800	0.08	47.71	2.09	Compl. φ
		0.12	21.57	1.22	Compl. φ
		0.14	8.50	0.69	Partial. φ
	900	0.08	42.45	2.59	Compl. φ
		0.12	13.67	0.69	Partial. φ
		0.14	-0.72	1.13	Not. φ
	1000	0.08	37.98	2.24	Compl. φ
		0.12	6.98	1.14	Partial. φ
		0.14	-8.53	1.25	Not. φ

Table A 5 Porosity, Brinell hardness and Build up rate values of AlSi10Mg+4Cu parallelepiped samples produced by LPBF (with rotated scanning strategy).

P [W]	*v* [mm/s]	h_d [mm]	*VED* [J/mm^3]	Build-up rate [cm^3/h]	$\rho_{Arch.}$ [Kg/dm^3]	$\rho_{Rel.}$ [%]	Porosity [%]	HB10
170	700	0.12	67.46	9.07	2.70	98.72	1.27	141.6 ± 1.6
	800		59.03	10.37	2.70	98.71	1.29	145.0 ± 2.2
	900		52.47	11.66	2.71	98.76	1.23	141.4 ± 1.1
	1000		47.22	12.96	2.71	98.84	1.15	148.6 ± 0.5
180	700		71.43	9.07	2.71	98.83	1.16	141.4 ± 1.8
	800		62.50	10.37	2.71	98.90	1.09	139.4 ± 1.9
	900		55.56	11.66	2.72	99.16	0.83	147.2 ± 2.0
	1000		50.00	12.96	2.71	99.03	0.96	149.2 ± 2.0
170	700	0.14	57.82	10.58	2.70	98.67	1.32	137.0 ± 2.3
	800		50.60	12.10	2.70	98.62	1.37	144.8 ± 3.1
	900		44.97	13.61	2.70	98.64	1.35	145.4 ± 2.6
	1000		40.48	15.12	2.71	98.97	1.02	148.4 ± 0.8
180	700		61.22	10.58	2.71	99.04	0.96	142.0 ± 2.1
	800		53.57	12.10	2.70	98.63	1.36	141.0 ± 1.2
	900		47.62	13.61	2.70	98.62	1.37	145.4 ± 1.3
	1000		42.86	15.12	2.71	98.95	1.05	147.4 ± 2.3

References

[1] D. Herzog, V. Seyda, E. Wycisk, C. Emmelmann, Additive manufacturing of metals, Acta Mater. 117 (2016) 371–392. doi:10.1016/j.actamat.2016.07.019.

[2] N. Li, S. Huang, G. Zhang, R. Qin, W. Liu, H. Xiong, G. Shi, J. Blackburn, Progress in additive manufacturing on new materials: A review, J. Mater. Sci. Technol. 35 (2018) 242–269. doi:10.1016/j.jmst.2018.09.002.

[3] T. DebRoy, H.L. Wei, J.S. Zuback, T. Mukherjee, J.W. Elmer, J.O. Milewski, A.M. Beese, A. Wilson-Heid, A. De, W. Zhang, Additive manufacturing of metallic components – Process, structure and properties, Prog. Mater. Sci. 92 (2018) 112–224. doi:10.1016/j.pmatsci.2017.10.001.

[4] G. Kasperovich, J. Haubrich, J. Gussone, G. Requena, Correlation between porosity and processing parameters in TiAl6V4 produced by selective laser melting, Mater. Des. 105 (2016) 160–170. doi:10.1016/j.matdes.2016.05.070.

[5] S. Liu, Y.C. Shin, Additive manufacturing of Ti6Al4V alloy: A review, Mater. Des. 164 (2018) 107552. doi:10.1016/j.matdes.2018.107552.

[6] D. Wang, C. Song, Y. Yang, Y. Bai, Investigation of crystal growth mechanism during selective laser melting and mechanical property characterization of 316L stainless steel parts, Mater. Des. 100 (2016) 291–299. doi:10.1016/j.matdes.2016.03.111.

[7] H. Choo, K.-L. Sham, J. Bohling, A. Ngo, X. Xiao, Y. Ren, P.J. Depond, M.J. Matthews, E. Garlea, Effect of laser power on defect, texture, and microstructure of a laser powder bed fusion processed 316L stainless steel, Mater. Des. 164 (2018) 107534. doi:10.1016/j.matdes.2018.12.006.

[8] V.A. Popovich, E. V. Borisov, A.A. Popovich, V.S. Sufiiarov, D. V. Masaylo, L. Alzina, Functionally graded Inconel 718 processed by additive manufacturing: Crystallographic texture, anisotropy of microstructure and mechanical properties, Mater. Des. 114 (2017) 441–449. doi:10.1016/j.matdes.2016.10.075.

[9] K. Kempen, L. Thijs, J. Van Humbeeck, J.-P. Kruth, Processing AlSi10Mg by selective laser melting: parameter optimisation and material characterisation, Mater. Sci. Technol. 31 (2015) 917–923. doi:10.1179/1743284714Y.0000000702.

[10] H. Rao, S. Giet, K. Yang, X. Wu, C.H.J. Davies, The influence of processing parameters on aluminium alloy A357 manufactured by Selective Laser Melting, Mater. Des. 109 (2016) 334–346.

doi:10.1016/j.matdes.2016.07.009.

[11] Y. Brif, M. Thomas, I. Todd, The use of high-entropy alloys in additive manufacturing, Scr. Mater. 99 (2015) 93–96. doi:10.1016/j.scriptamat.2014.11.037.

[12] J.H. Martin, B.D. Yahata, J.M. Hundley, J.A. Mayer, T.A. Schaedler, T.M. Pollock, 3D printing of high-strength aluminium alloys, Nature. 549 (2017) 365–369. doi:10.1038/nature23894.

[13] S.A.M. Tofail, E.P. Koumoulos, A. Bandyopadhyay, S. Bose, L. O'Donoghue, C. Charitidis, Additive manufacturing: scientific and technological challenges, market uptake and opportunities, Mater. Today. 21 (2018) 22–37. doi:10.1016/j.mattod.2017.07.001.

[14] J.H. Tan, W.L.E. Wong, K.W. Dalgarno, An overview of powder granulometry on feedstock and part performance in the selective laser melting process, Addit. Manuf. 18 (2017) 228–255. doi:10.1016/j.addma.2017.10.011.

[15] A.T. Sutton, C.S. Kriewall, M.C. Leu, J.W. Newkirk, Powder characterisation techniques and effects of powder characteristics on part properties in powder-bed fusion processes, Virtual Phys. Prototyp. 12 (2017) 3–29. doi:10.1080/17452759.2016.1250605.

[16] F. Calignano, G. Cattano, D. Manfredi, Manufacturing of thin wall structures in AlSi10Mg alloy by laser powder bed fusion through process parameters, J. Mater. Process. Technol. 255 (2018) 773–783. doi:10.1016/j.jmatprotec.2018.01.029.

[17] M. Krishnan, E. Atzeni, R. Canali, F. Calignano, D. Manfredi, E.P. Ambrosio, L. Iuliano, On the effect of process parameters on properties of AlSi10Mg parts produced by DMLS, Rapid Prototyp. J. 20 (2014) 449–458. doi:10.1108/RPJ-03-2013-0028.

[18] J. Sun, Y. Yang, D. Wang, Parametric optimization of selective laser melting for forming Ti6Al4V samples by Taguchi method, Opt. Laser Technol. 49 (2013) 118–124. doi:10.1016/j.optlastec.2012.12.002.

[19] N. Read, W. Wang, K. Essa, M.M. Attallah, Selective laser melting of AlSi10Mg alloy: Process optimisation and mechanical properties development, Mater. Des. 65 (2015) 417–424. doi:10.1016/j.matdes.2014.09.044.

[20] Z. Li, I. Kucukkoc, D.Z. Zhang, F. Liu, Optimising the process parameters of selective laser melting for the fabrication of Ti6Al4V alloy, Rapid Prototyp. J. 24 (2018) 150–159. doi:10.1108/RPJ-03-2016-0045.

[21] D. Gu, Y. Shen, Balling phenomena during direct laser sintering of multi-component Cu-based metal powder, J. Alloys Compd. 432 (2007) 163–166. doi:10.1016/j.jallcom.2006.06.011.

[22] I. Yadroitsev, I. Smurov, Selective laser melting technology: From the single laser melted track stability to 3D parts of complex shape, Phys. Procedia. 5 (2010) 551–560. doi:10.1016/j.phpro.2010.08.083.

[23] C. Li, Y.B. Guo, J.B. Zhao, Interfacial phenomena and characteristics between the deposited material and substrate in selective laser melting Inconel 625, J. Mater. Process. Technol. 243 (2017) 269–281. doi:10.1016/j.jmatprotec.2016.12.033.

[24] P. Wei, Z. Wei, Z. Chen, J. Du, Y. He, J. Li, Y. Zhou, The AlSi10Mg samples produced by selective laser melting: single track, densification, microstructure and mechanical behavior, Appl. Surf. Sci. 408 (2017) 38–50. doi:10.1016/j.apsusc.2017.02.215.

[25] A. Aversa, M. Moshiri, E. Librera, M. Hadi, G. Marchese, D. Manfredi, M. Lorusso, F. Calignano, S. Biamino, M. Lombardi, M. Pavese, Single scan track analyses on aluminium based powders, J. Mater. Process. Technol. 255 (2018) 17–25. doi:10.1016/j.jmatprotec.2017.11.055.

[26] X. Nie, H. Zhang, H. Zhu, Z. Hu, L. Ke, X. Zeng, Analysis of processing parameters and characteristics of selective laser melted high strength Al-Cu-Mg alloys: From single tracks to cubic samples, J. Mater. Process. Technol. 256 (2018) 69–77. doi:10.1016/j.jmatprotec.2018.01.030.

[27] N.T. Aboulkhair, N.M. Everitt, I. Ashcroft, C. Tuck, Reducing porosity in AlSi10Mg parts processed by selective laser melting &, Addit. Manuf. 1–4 (2014) 77–86. doi:10.1016/j.addma.2014.08.001.

[28] H. Yeung, B.M. Lane, M.A. Donmez, J.C. Fox, J. Neira, Implementation of Advanced Laser Control Strategies for Powder Bed Fusion Systems, Procedia Manuf. 26 (2018) 871–879. doi:10.1016/j.promfg.2018.07.112.

[29] ASTM B962, Standard Test Methods for Density of Compacted or Sintered Powder Metallurgy (PM) Products Using Archimedes Principle, ASTM Int. (2013) 1–7. doi:10.1520/B0962-13.2.

[30] D.R. Askeland, P.P. Fulay, W.J. Wright, The science and engineering of materials, Third S.I., 1998.

[31] D. Manfredi, F. Calignano, M. Krishnan, R. Canali, E.P. Ambrosio, E. Atzeni, From powders to dense metal parts: Characterization of a commercial alsimg alloy processed through direct metal laser sintering, Materials (Basel). 6 (2013) 856–869. doi:10.3390/ma6030856.

[32] ASTM E10-18, Standard Test Method for Brinell Hardness of Metallic Materials, ASTM Int. (2012) 1–36. doi:10.1520/E0010-15.

[33] K. Kempen, L. Thijs, E. Yasa, M. Badrossamay, W. Verheecke, J.P. Kruth, Process Optimization and micostructural analysis for Selective Laser Melting of AlSi10Mg, Solid Free. Fabr. (2011) 484–495.

[34] A. Aversa, M. Lorusso, G. Cattano, D. Manfredi, F. Calignano, E.P. Ambrosio, S. Biamino, P. Fino, M. Lombardi, M. Pavese, A study of the microstructure and the mechanical properties of an AlSiNi alloy produced via selective laser melting, J. Alloys Compd. 695 (2016) 1–9. doi:10.1016/j.jallcom.2016.10.285.

[35] P. Wang, K.G. Prashanth, S. Pauly, J. Eckert, S. Scudino, Microstructure and mechanical properties of Al-Cu alloys fabricated by selective laser melting of powder mixtures, 735 (2018) 2263–2266. doi:10.1016/j.jallcom.2017.10.168.

[36] E.O. Olakanmi, R.F. Cochrane, K.W. Dalgarno, Densification mechanism and microstructural evolution in selective laser sintering of Al-12Si powders, J. Mater. Process. Technol. 211 (2011) 113–121. doi:10.1016/j.jmatprotec.2010.09.003.

[37] M. Badrossamay, E. Yasa, J. Van Vaerenbergh, J.P. Kruth, Improving productivity rate in SLM of commercial steel powders, in: S. of M. Engineers (Ed.), Schaumburg, IL, USA, 2009: pp. 1–13.

[38] P. Mercelis, J.P. Kruth, Residual stresses in selective laser sintering and selective laser melting, Rapid Prototyp. J. 12 (2006) 254–265. doi:10.1108/13552540610707013.

[39] K. Bartkowiak, S. Ullrich, T. Frick, M. Schmidt, New developments of laser processing aluminium alloys via additive manufacturing technique, Phys. Procedia. 12 (2011) 393–401. doi:10.1016/j.phpro.2011.03.050.

[40] A. Aversa, F. Bosio, S. Marola, M. Lorusso, D. Manfredi, L. Battezzati, P. Fino, M. Lombardi, Laser Single Scan Tracks of New Aluminium Alloys Compositions, Proc. EURO PM2018. (2018) 1–6. doi:https://iris.polito.it/handle/11583/2715552.

[41] D. Gu, Y. Shen, Balling phenomena in direct laser sintering of stainless steel powder: Metallurgical mechanisms and control methods, Mater. Des. 30 (2009) 2903–2910. doi:10.1016/j.matdes.2009.01.013.

[42] I. Yadroitsev, A. Gusarov, I. Yadroitsava, I. Smurov, Single track formation in selective laser melting of metal powders, J. Mater. Process. Technol. 210 (2010) 1624–1631. doi:10.1016/j.jmatprotec.2010.05.010.

[43] F. Calignano, D. Manfredi, E.P. Ambrosio, L. Iuliano, P. Fino, Influence of process parameters on surface roughness of aluminum parts produced by DMLS, Int. J. Adv. Manuf. Technol. 67 (2013) 2743–2751. doi:10.1007/s00170-012-4688-9.